Quantification of Restitution Dispersion From the Dynamic Changes of the T-Wave Peak to End, Measured at the Surface ECG

Ana Mincholé*, Esther Pueyo, José Felix Rodríguez, Ernesto Zacur, Manuel Doblaré, and Pablo Laguna

***Abstract*—Action potential duration restitution (APDR) curves present spatial variations due to the electrophysiological heterogeneities present in the heart. Enhanced spatial APDR dispersion in ventricle has been suggested as an arrhythmic risk marker. In this study, we propose a method to noninvasively quantify dispersion of APDR slopes at tissue level by making only use of the surface electrocardiogram (ECG). The proposed estimate accounts for rate normalized differences in the steady-state T-wave peak to T-wave end interval (T_{pe}). A methodology is developed for its computation, which includes compensation for the T_{pe} memory lag after heart-rate (HR) changes. The capability of the proposed estimate to reflect APDR dispersion is assessed using a combination of ECG signal processing, and computational modeling and simulation. Specifically, ECG recordings of control subjects undergoing a tilt test trial are used to measure that estimate, while its capability to provide a quantification of APDR dispersion at tissue level is assessed by using a 2-D ventricular tissue simulation. From this simulation, APDR dispersion, denoted as $\Delta\alpha^{\mathrm{SIM}}$, is calculated, and pseudo-ECGs are derived. Estimates of APDR dispersion measured from the pseudo-ECGs show to correlate with $\Delta\alpha^{\mathrm{SIM}}$, being the mean relative error below 5%. A comparison of the ECG estimates obtained from tilt test recordings and the $\Delta\alpha^{\mathrm{SIM}}$ values measured *in silico* simulations at tissue level show that differences between them are below 20%, which is within physiological variability limits. Our results provide evidence that the proposed estimate is a noninvasive measurement of APDR dispersion in ventricle. Additional results from this study confirm that T_{pe} adapts to HR changes much faster than the QT interval.**

***Index Terms*—Rate adaptation, repolarization dispersion, restitution dispersion, T-wave peak to T-wave end.**

I. Introduction

HEART-RATE (HR) dependence of action potential duration (APD), also called restitution kinetics, is thought to be critical in activation instability and, therefore, provides relevant information for ventricular arrhythmic risk stratification [1], [2]. The dynamic APD restitution (APDR) curve, measured using the so-called dynamic restitution protocol, quantifies the relationship between the APD and the RR interval (inverse of HR) at steady-state when pacing at different RR values [3], [4]. Despite the large number of studies in the literature on the role of steep APDR curves in the development of ventricular arrhythmias [4], [5], it is unlikely that the conditions of constant rapid pacing used to experimentally characterize that relationship apply to the clinical situation. Heterogeneities in the ventricle lead to non uniform restitution properties, which makes APDR curves present spatial variations [6]. Dispersion is a measure of that spatial variation. Recent studies have suggested that dispersion in the APDR curves may act as a potent arrhythmogenic substrate [7], [8], and increments in that dispersion have been associated with greater propensity to suffer from ventricular tachycardia/fibrillation [9].

The main limitation on the usability of APDR dispersion as a risk index is that its quantification requires invasive procedures [10]. In this study we propose a method to indirectly estimate dispersion of restitution slopes by making only use of the surface electrocardiogram (ECG). We propose an ECG measure that quantifies dispersion in the dynamic APDR slopes by characterizing the relationship between the distance from T-wave peak to T-wave end (T_{pe}) and the RR interval under different stationary conditions.

T_{pe} interval is generally accepted to reflect differences in the time for completion of repolarization at different regions in the ventricle. Some studies have proposed that T_{pe} is an index of transmural dispersion of repolarization [11], while others have claimed that T_{pe} does not correlate only with transmural

Manuscript received August 5, 2010; revised October 19, 2010; accepted November 16, 2010. Date of publication December 30, 2010; date of current version April 20, 2011. This work was supported in part by the Ministerio de Ciencia y Tecnología, Spain, under Project TEC2010-19410 and Project TEC2010-21703-C03-02, in part by the Diputación General de Aragón (DGA), Spain, under Grupos Consolidados GTC ref:T30, PI165/09, and PI 144/2009, in part by the ISCIII, Spain, and through the Center for International Business Education and Research (CIBER) CB06/01/0062, and in part by the Royal Society International Joint Project. *Asterisk indicates corresponding author.*

*A. Mincholé is with the Centro de Investigación Biomédica en Red (CIBER) de Bioingeniería, Biomateriales y Nanomedicina (CIBER-BBN), and the Communications Technology Group (GTC), Aragón Institute of Engineering Research (I3A), University of Zaragoza, Zaragoza 50015, Spain (e-mail: minchole@unizar.es).

E. Pueyo and P. Laguna are with the Centro de Investigación Biomédica en Red (CIBER) de Bioingeniería, Biomateriales y Nanomedicina (CIBER-BBN), and the Communications Technology Group (GTC), Aragón Institute of Engineering Research (I3A), University of Zaragoza, Zaragoza 50015, Spain (e-mail: epueyo@unizar.es; laguna@unizar.es).

J. F. Rodríguez and M. Doblaré are with the Structural Mechanics and Material Modeling Group (GEMM), Aragón Institute of Engineering Research (I3A), and the Centro de Investigación Biomédica en Red (CIBER) de Bioingeniería, Biomateriales y Nanomedicina (CIBER-BBN), University of Zaragoza, Zaragoza 50015, Spain (e-mail: jfrodrig@unizar.es; doblare@unizar.es).

E. Zacur is with the Communications Technology Group (GTC), Aragón Institute of Engineering Research (I3A), University of Zaragoza, Zaragoza 50015, Spain (e-mail: zacur@unizar.es).

Color versions of one or more of the figures in this paper are available online at http://ieeexplore.ieee.org.

Digital Object Identifier 10.1109/TBME.2010.2097597

dispersion of repolarization but it also includes other heterogeneities, such as apicobasal ones [12], [13].

Each value of the APDR curve represents a stationary state corresponding to a specific HR value, and, therefore, the ECG measurement proposed to estimate restitution dispersion should in principle be computed using ECG segments of stable HR regimes. Since those type of segments are difficult to get in clinical practice, we propose a methodology that overcomes that restriction by modeling the dependence of the T_{pe} interval on a history of previous RR intervals and compensating for the T_{pe} memory lag. This model has been previously used to characterize rate adaptation of the QT interval [14], which has been known to adapt, similarly as does the APD, in two phases: a fast initial one and a subsequent slow accommodation [3], [15], [16]. Previous studies characterizing T_{pe} rate dependence are controversial, with T_{pe} shown to be independent of HR by some authors [17] and markedly HR dependent by others [18]. In this study we characterize T_{pe} rate adaptation, and compare it with QT rate adaptation.

Our proposed ECG-based estimate of APDR slope dispersion, is evaluated on a database of ECG recordings from healthy subjects undergoing a tilt test trial. In this trial, step-like HR changes are generated, which are used in this study to measure dynamic changes of the T_{pe}, and compute the proposed estimate.

The capability of the proposed ECG measurement to provide estimates of APDR slope dispersion at tissue level has been assessed by simulating electrical propagation in a 2-D tissue representing a slice across the human left ventricular wall, and computing pseudo-ECGs. An electrophysiologically detailed human ventricular cell model [19] is used to generate action potentials. Pacings at different RR intervals are simulated to compute dynamic APDR curves, and eventually APDR slope dispersion.

A comparison of the proposed ECG estimate evaluated from the simulated pseudo-ECGs and from the tilt test ECG recordings shows that simulated data is in good agreement with clinical/experimental data. Additionally, using the 2-D simulated data we confirm that the proposed ECG estimate is a measure of APDR slope dispersion at tissue level.

The manuscript is outlined as follows. Section II presents the database and the method used to estimate APDR slope dispersion from the surface ECG and describes the 2-D tissue modeling and simulation. Section III contains the results that show the capability of the proposed ECG measurement to provide estimates of the APDR slope dispersion. Sections IV and V present the discussion and the main limitations of the study. Section VI summarizes the conclusions.

II. Materials and Methods

This section mainly includes the quantification of APDR dispersion from ECG-based estimates; and the introduction of a 2-D modeling and simulation to assess the proposed estimates. Section II-A introduces the data and ECG signal processing delineation procedures. In Section II-B, the relationship between ventricular APDR slope dispersion, denoted by $\Delta\alpha$, and its surface ECG estimate, denoted by $\widehat{\Delta\alpha}^{\mathrm{ECG_s}}$, is presented for the case of stable RR segments (see Fig. 1, left). Hereinafter, "the hat" ($\widehat{\ }$) refers to estimates from the ECG. The difficulty of getting stable RR segments made us propose a methodology to compensate for the T_{pe} memory lag after HR changes (see Section II-C), and use it in the derivation of the ECG estimate for APDR slope dispersion for the case of unstable RR segments, denoted by $\widehat{\Delta\alpha}^{\mathrm{ECG_c}}$. In Section II-D, the 2-D ventricular tissue model used to evaluate the extent to which ECG estimates reflect the underlying restitution dispersion is described. Simulated APDR dispersion from the 2-D model, denoted by $\Delta\alpha^{\mathrm{SIM}}$, and its corresponding estimate measured from the pseudo-ECG, $\widehat{\Delta\alpha}^{\mathrm{pECG}}$, are computed (see Fig. 1, right).

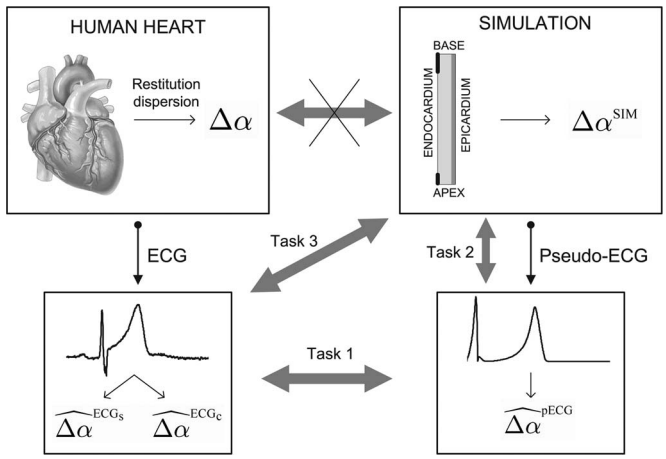

Fig. 1. Outline of the methods used in this study. Crossed arrow shows a desirable but unaccessible connection. Tasks 1, 2, and 3 represent the different comparison tasks to be done in Section III (see Section III-A– D for details).

A. Population and ECG Delineation

Fifteen volunteers (11 males, 4 females) from 25 to 33 years old, without any previous history of cardiovascular disease, have undergone a head-up tilt test trial according to the following protocol: 4 min in the supine position, 5 min in the standing position tilted head-up to an angle of 70°, and 4 min back to the supine position. The protocol generates two step-like RR changes with stabilized RR intervals after each of them. 12-lead ECGs are recorded during the whole test at a sampling frequency of 1000 Hz.

ECG delineation is performed using a wavelet-based delineator [20]. In each subject, the lead with the highest SNR, estimated as the maximum T-wave amplitude over the rms value of the high-frequency noise (above 25 Hz) of the interval between the ST segment to the end of the *P*-wave, is selected. In our database, leads V2, V3, or V4 have always been the leads with highest SNR. RR, QT, and T_{pe} intervals are computed from the ECG delineation marks in the selected lead, after visually examining and removing the erroneous delineation marks.

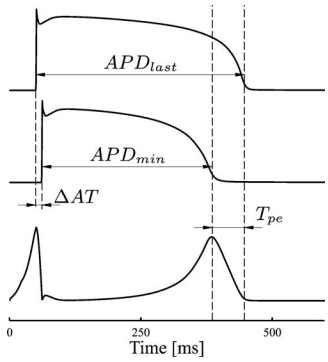

Fig. 2. Representation of the T_{pe} interval in terms of APDs and delay of activation times (ΔAT).

B. Quantification of Restitution Dispersion Using Stable RR Segments of the Surface ECG

We propose a method to indirectly compute dispersion in dynamic APDR slopes within the ventricle, by making only use of the surface ECG (see Fig. 1, bottom-left).

T_{pe} interval reflects differences in the time for completion of repolarization by different cells spanning the ventricular wall. Therefore, and based on [8] and [11], the T_{pe} interval can be expressed in terms of APDs as follows:

$$T_{pe} = \mathrm{APD}_{\mathrm{last}} - \mathrm{APD}_{\mathrm{min}} - \Delta\mathrm{AT} \tag{1}$$

where $\mathrm{APD}_{\mathrm{min}}$ corresponds to the cell with the minimum APD among those which are currently repolarizing at the T-wave peak instant (time instant when the maximum repolarization gradient sum occurs) and $\mathrm{APD}_{\mathrm{last}}$ is the APD of the last cell to repolarize. ΔAT represents the activation time delay between both cells with $\mathrm{APD}_{\mathrm{min}}$ and $\mathrm{APD}_{\mathrm{last}}$, as shown in Fig. 2. Note that in this work Δ is considered as a difference operator, which is applied in this case to activation times at two spatial sites. This ΔAT delay hardly changes with RR for RR intervals above 600 ms [19], [21]. Therefore, changes in the T_{pe} under variations of the RR interval can be obtained as

$$\frac{\partial T_{pe}}{\partial RR} = \frac{\partial \mathrm{APD}_{\mathrm{last}}}{\partial RR} - \frac{\partial \mathrm{APD}_{\mathrm{min}}}{\partial RR} \tag{2}$$

where $\partial\Delta\mathrm{AT}/\partial RR$ has been neglected, under the premise that RR intervals above 600 ms are considered.

If we restrict (2) to the dynamic protocol, where each value of the APDR curve represents a steady-state APD value (see Fig. 3), and the regions with $\mathrm{APD}_{\mathrm{min}}$ and $\mathrm{APD}_{\mathrm{last}}$ remain fixed when varying RR, then

$$\frac{\partial T_{pe}^{\mathrm{dyn}}}{\partial RR} = \frac{\partial \mathrm{APD}_{\mathrm{last}}^{\mathrm{dyn}}}{\partial RR} - \frac{\partial \mathrm{APD}_{\mathrm{min}}^{\mathrm{dyn}}}{\partial RR} \tag{3}$$

where T_{pe}^{dyn} and $\mathrm{APD}^{\mathrm{dyn}}$ refer to the steady values of T_{pe} and APD for each RR interval. Hereinafter, the superindex "dyn" refers to the dynamic protocol. In case of having only pairs of steady-state values, $[RR, T_{pe}^{\mathrm{dyn}}]$, the derivatives in (3) may be approximated by increments Δ

$$\frac{\partial T_{pe}^{\mathrm{dyn}}}{\partial RR} \approx \frac{\Delta T_{pe}^{\mathrm{dyn}}}{\Delta RR} \tag{4}$$

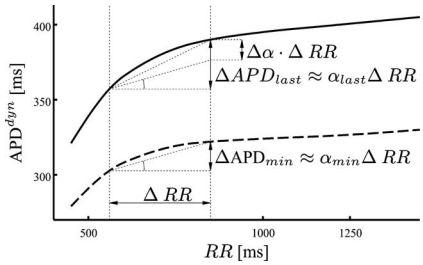

Fig. 3. Dynamic restitution curves (APDR) for two regions corresponding to $\mathrm{APD}_{\mathrm{min}}$ (dashed line) and $\mathrm{APD}_{\mathrm{last}}$ (solid line). Slopes α_{min} and α_{last} are estimated for a change in the RR interval.

where $\Delta T_{pe}^{\mathrm{dyn}}$ and ΔRR represent the variations in T_{pe} and RR, respectively, *between two stable ECG segments at different RR intervals*.

If we let α_{last} and α_{min} denote the slopes of the dynamic restitution curves at the regions corresponding to $\mathrm{APD}_{\mathrm{last}}$ and $\mathrm{APD}_{\mathrm{min}}$, respectively:

$$\alpha_i = \frac{\partial \mathrm{APD}_i^{\mathrm{dyn}}}{\partial RR} \quad \text{where } i = \{\text{last,min}\} \tag{5}$$

the spatial difference $\Delta\alpha = (\alpha_{\mathrm{last}} - \alpha_{\mathrm{min}})$ (see Fig. 3), which measures dispersion of restitution slopes, can be estimated from the ECG by introducing (5) into (3) and (4), resulting in

$$\widehat{\Delta\alpha}^{\mathrm{ECG_s}} = \frac{\Delta T_{pe}^{\mathrm{dyn}}}{\Delta RR} \tag{6}$$

where the superindex "ECG$_s$" indicates that quantification of restitution dispersion is done by using stable ECG segments, as required in the dynamic protocol, at two different RR intervals. Δ at left-hand side of (6) refers to a difference of restitution slopes occurring at two regions, while both Δ at right-hand side refer to beat interval differences associated with two RR levels.

Note that in cases of, e.g., ventricular wedges, where T_{pe} *includes only transmural heterogeneities*, $\mathrm{APD}_{\mathrm{last}}$ and $\mathrm{APD}_{\mathrm{min}}$ would correspond to APDs at the midmyocardium and epicardium, respectively, and therefore, $\widehat{\Delta\alpha}^{\mathrm{ECG_s}}$ would represent an estimation of transmural dispersion of restitution slopes.

C. Quantification of Restitution Dispersion Using Unstable RR Segments of the Surface ECG

Stable RR segments, needed to measure the rate related increment $\Delta T_{pe}^{\mathrm{dyn}}$ in (6), are difficult to get in the clinical practice. In order to overcome this limitation, we propose a methodology to compensate for the T_{pe} memory lag after RR changes.

The model shown in Fig. 4, previously proposed to quantify QT rate adaptation [14], is used to characterize the T_{pe} dependence on RR. The input $x_{\mathrm{RR}}(n)$ and output $y_{\mathrm{T}_{pe}}(n)$ denote the RR and T_{pe} series of each recording after interpolation and resampling to a sampling frequency of $f_s = 1$ Hz.

Impulse response $\mathbf{h} = [h(1), \ldots, h(N)]^T$ includes information about the memory of the system, that is, a characterization of the influence of a history of previous RR intervals on each T_{pe} measurement. Therefore, $z_{\mathrm{RR}}(n)$ represents a surrogate of $x_{\mathrm{RR}}(n)$ with the memory effect of T_{pe} compensated for. The

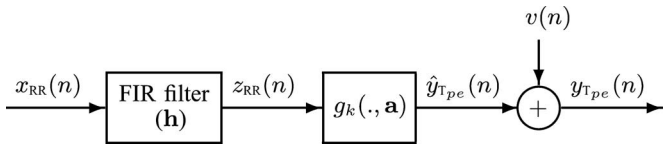

Fig. 4. Block diagram describing the $[RR, T_{pe}]$ relationship consisting of a time invariant FIR filter (impulse response $\mathbf{h}$) and a nonlinear function $g_k(.,\mathbf{a})$ described by the parameter vector $\mathbf{a}$. $v(n)$ accounts for the output error.

length N of vector $\mathbf{h}$ was set to 150 samples that correspond to 150 s, which widely exceeds the T_{pe} memory lag for the data population used in this study. The function $g_k(.,\mathbf{a})$, dependent on the parameter vector $\mathbf{a} = [a(0), a(1)]^T$, represents the relationship between the RR interval and the T_{pe} interval once the memory effect has been compensated for (i.e. under stationary conditions). Ten different biparametric regression models that span from a linear to a hyperbolic relationship, as described in [14], are considered for $g_k(.,\mathbf{a})$, and the one that best fits the data of each subject is identified.

The estimated output $\hat{y}_{\mathrm{T}_{pe}}(n)$ is defined as

$$\hat{y}_{\mathrm{T}_{pe}}(n) = g_k(z_{\mathrm{RR}}(n), \mathbf{a}) \tag{7}$$

where, in vector notation, $\mathbf{z}_{\mathrm{RR}}$, is the convolution between the input vector $\mathbf{x}_{\mathrm{RR}}$ and the impulse response ($\mathbf{z}_{\mathrm{RR}} = \mathbf{x}_{\mathrm{RR}} * \mathbf{h}$).

The optimum values of the FIR filter response $\mathbf{h}$, vector $\mathbf{a}$, and function g_k are searched for, by minimizing the difference between the estimated output $\hat{y}_{\mathrm{T}_{pe}}(n)$ (see (7)) and the T_{pe} interval series $y_{\mathrm{T}_{pe}}(n)$, for each subject independently using the whole recording. The estimator used for the optimization is a regularized least-square estimator

$$\{\mathbf{h}^*, \mathbf{a}^*, k^*\} = \arg \min_{\{\mathbf{h},\mathbf{a},k\}} \left(\left\| \mathbf{y}_{\mathrm{T}_{pe}} - \hat{\mathbf{y}}_{\mathrm{T}_{pe}} \right\|^2 + \beta^2 \left\| \mathbf{D}\mathbf{h} \right\|^2 \right) \tag{8}$$

where $\mathbf{D}$ is a regularization matrix that penalizes the fact that $\mathbf{h}$ deviates from having an exponential decay [16], and β is the regularization parameter whose value is obtained by using the "L-curve" criterion [22]. In the cost function, $\mathbf{y}_{\mathrm{T}_{pe}}$ and $\hat{\mathbf{y}}_{\mathrm{T}_{pe}}$ are the signals expressed in vector notation. With the computed value for β, the optimum values, $\mathbf{h}^*$ and $\mathbf{a}^*$ in (8), are determined by using a "quasi-Newton" optimization technique described in [23], subject to two constraints: the sum of the $\mathbf{h}$ components is 1 ($\sum_{i=1}^{N} h(i) = 1$), to ensure normalized filter gain, and all the components of $\mathbf{h}$ are nonnegative ($h(i) \geq 0$), to give a physiological plausible interpretation. Regarding k^* in (8), in order to account for the inter-subject variability in the $[RR, T_{pe}]$ relationship, the regression function $g_k(.,\mathbf{a})$ is determined as the one that minimizes the mean square error for each subject independently.

After $\mathbf{h}$ and $g_k(.,\mathbf{a})$ have been optimized, we can make use of $z_{\mathrm{RR}}(n)$ as a surrogate of the running RR series that would generate a truly stationary period in the running repolarization interval T_{pe}. Then, the i th pair $[z_{\mathrm{RR}}(i), T_{pe}(i)]$ represents the surrogate for the RR interval and the T_{pe} interval measured in an stable ECG segment. Therefore, the estimate of restitution dispersion derived in (6) can be replaced with the following equation, obtained by differentiating (7) with respect to z_{RR}

$$\widehat{\Delta\alpha}^{\mathrm{ECG_c}} = \left. \frac{\partial T_{pe}}{\partial z_{\mathrm{RR}}} \right|_{z_{\mathrm{RR}} = \bar{z}_{\mathrm{RR}}} = \left. \frac{\partial g_k(z_{\mathrm{RR}}, \mathbf{a})}{\partial z_{\mathrm{RR}}} \right|_{z_{\mathrm{RR}} = \bar{z}_{\mathrm{RR}}} . \tag{9}$$

The above expression has the advantage of avoiding the need for stationary ECG segments. The superindex "ECG_c" indicates that the quantification of restitution dispersion from the ECG is done by compensating for the T_{pe} memory lag using the model described in Fig. 4. This estimate is a robust alternative to $\widehat{\Delta\alpha}^{\mathrm{ECG_s}}$ (see Fig. 1, bottom-left). In (9), the derivative is evaluated at the mean z_{RR} value, $\bar{z}_{\mathrm{RR}}$, of the complete recording.

Additionally, T_{pe} rate dependence is characterized using the model of Fig. 4. The time required for T_{pe} to complete 90% of its rate adaptation, denoted by t_{90}, is computed by setting a threshold of 0.1 to the cumulative sum of the filter impulse response, $c(n)$

$$c(n) = \sum_{i=n}^{N} h(i), \quad \text{leading to}$$

$$t_{90} = \frac{1}{f_s} \arg\max_n \left(c(n) > 0.1 \right). \tag{10}$$

An analogous procedure is used to calculate t_{70}, t_{50} and t_{25} by replacing the threshold 0.1 in (10), with 0.3, 0.5, and 0.75, respectively. The adaptation rate is quantified as $r(n) = [1 - c(n)] \cdot 100$, which represents the percentage of the total T_{pe} adaptation reached at time instant n.

D. Computational Modeling and Simulation

Computational modeling and simulation is used in this study to assess how the proposed estimates evaluated from the ECG, $\widehat{\Delta\alpha}^{\mathrm{ECG_s}}$ and $\widehat{\Delta\alpha}^{\mathrm{ECG_c}}$, represent dispersion of the APDR slopes at tissue level (see Fig. 1, right).

Propagation of the electrical activity in a left ventricular 2-D tissue slice is simulated using the human ten Tusscher action potential model [19], with numerical integration performed as described in [24]. The ten Tusscher model [19] describes the principal ionic currents through the cardiac cell membrane with high degree of electrophysiological detail for the three types of cells in the ventricular wall: endocardial, midmyocardial and epicardial cells. The 2-D tissue slice used in this study is 7.5 cm long by 1 cm wide, representing the base to apex and the endocardial to epicardial distances, respectively, as shown in Fig. 5. Conductivity of the tissue along the fiber direction is set to σ_L = 0.0013 mS with a membrane capacitance of 1 μF/cm^2, obtaining a maximum conduction velocity of 71 cm/s. Perpendicular to the fiber direction, the conductivity is 60% lower, σ_T = 0.00052 mS, resulting in a conduction velocity of 42 cm/s, which is comparable to the average velocity of 44 cm/s recorded *in vivo* and across the arterially perfused transmural wedge preparation [25]. A transmural linear variation of the helix fiber angle from +60° at the endocardium to –60° at the epicardium is assumed based on [26].

As illustrated in Fig. 5, two areas in the subendocardium are stimulated simultaneously: 1 cm at the top of the base and 0.5 cm at the bottom of the apex, based on the activation

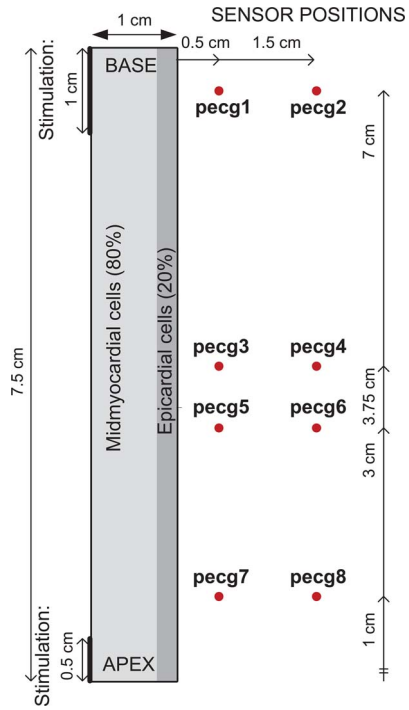

Fig. 5. Two-dimensional tissue slice used in the simulation, with indication of the default cell type distribution across the ventricular wall, and sensor positions used for pseudo-ECG computation.

sequence reported for an isolated human heart in [27]. Transmural heterogeneities are included in the 2-D tissue preparation by using two cell types: midmyocardial and epicardial cells. In order to match the complete activation sequence of [27] and to account for the influence of Purkinje fibers, endocardial cells in the simulated preparation are replaced with midmyocardial cells, known to have longer APDs. This is justified by the fact that Purkinje cells have longer APDs than midmyocardial cells and much longer than endocardial cells. The coupling between Purkinje and endocardium makes endocardial cells enlarge their action potentials [25], leading to APDs values similar to those simulated in our preparation. The APD in the different regions across the 2-D tissue slice are in agreement with the range reported in [28], where left ventricular wedge preparations from nonfailing human hearts were optically mapped.

The distribution of cell types in the simulated tissue are 80% of midmyocardial cells and 20% of epicardial cells [29]. To represent possible heterogeneities in human hearts and measure a range of plausible restitution dispersion values, the effect of varying the percentages of cell types within the ventricular wall is evaluated by considering additional distributions of 65%/35% and 90%/10% of midmyocardial/epicardial cells. For each cell type distribution, APDR curves are computed by pacing the 2-D tissue preparation at different RR intervals, following the so-called dynamic restitution protocol [4]. Dispersion of APDR slopes at tissue level is denoted by $\Delta\alpha^{\mathrm{SIM}}$ and is computed from the results of the 2-D simulation as follows:

$$\Delta\alpha^{\mathrm{SIM}} = \frac{\partial \mathrm{APD}^{\mathrm{dyn}}_{\mathrm{last}}}{\partial RR} - \frac{\partial \mathrm{APD}^{\mathrm{dyn}}_{\mathrm{min}}}{\partial RR} \tag{11}$$

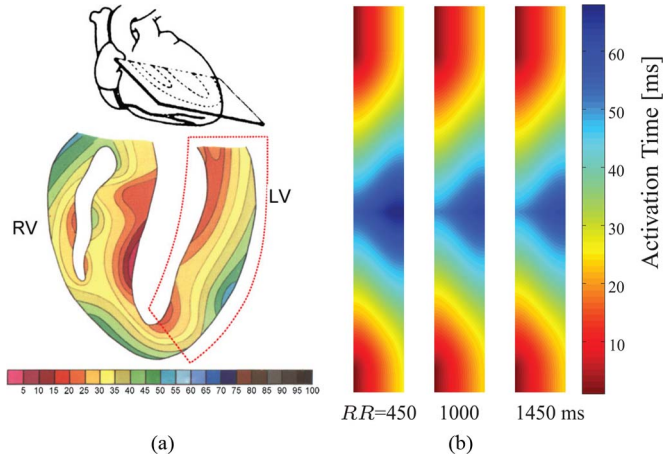

Fig. 6. Isochronic representation (in milliseconds) of ventricular activation: (a) experiment results reproduced from [27]; (b) 2-D tissue simulations when pacing at RR intervals of 450, 1000, and 1450 ms.

where $\mathrm{APD}^{\mathrm{dyn}}_{\mathrm{min}}$ and $\mathrm{APD}^{\mathrm{dyn}}_{\mathrm{last}}$ are defined as described in Section II-B. Estimations of $\Delta\alpha^{\mathrm{SIM}}$ are computed from pseudo-ECGs using (6). The pseudo-ECGs, each one measuring the extracellular potential at one of the sensor positions shown in Fig. 5 (Fig. 1, bottom-right), are computed as in [30]. The corresponding estimations are:

$$\widehat{\Delta\alpha}^{\mathrm{pECG}} = \frac{\partial T^{\mathrm{dyn}}_{pe}}{\partial RR} \tag{12}$$

where T^{dyn}_{pe} represents the T_{pe} interval measured from one of the pseudo-ECGs using the dynamic protocol.

III. Results

This section presents the different comparison tasks shown in Fig. 1. In Section III-A, the 2-D ventricular model is evaluated, with APDR estimates measured from pseudo-ECGs checked to be within the physiological range measured from ECG recordings (see task 1 in Fig. 1). In Section III-B, the capability of the proposed estimate measured from the pseudo-ECG ($\widehat{\Delta\alpha}^{\mathrm{pECG}}$) to quantify APDR dispersion at tissue level is assessed (see task 2 in Fig. 1). In Section III-C, ECG estimates evaluated in tilt test recordings and APDR dispersion $\Delta\alpha^{\mathrm{SIM}}$ are compared (see task 3 in Fig. 1). Additionally, Section III-D provides a characterization of T_{pe} rate adaptation.

A. Evaluation of the 2-D Simulations: Comparison Between Pseudo-ECGs and Clinical ECGs

The human ventricular model used in this study has been shown to reproduce experimentally observed data on APD restitution in single cells from the endo, epi, and midmyocardial regions of the ventricle [31]. Also, conduction velocity restitution measured in a 1-D cable of cells has been validated using experimental data [31].

The 2-D tissue preparation built in this study yields an activation sequence that is in good agreement with the experimental results reported in [27], as illustrated in Fig. 6. Simulated

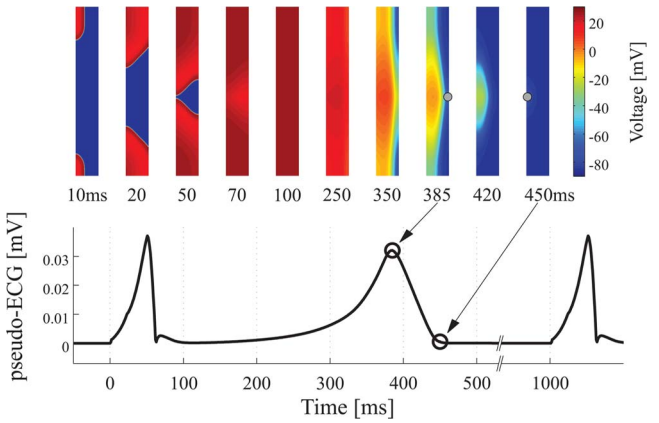

Fig. 7. (Top panel) Simulated sequence of isochronic voltage representation during steady-state pacing at 1000 ms. The position of the two cells corresponding to $\mathrm{APD}_{\mathrm{min}}$ for the peak of the T-wave and $\mathrm{APD}_{\mathrm{last}}$ for the end of the T-wave, are shown with a gray point. (Bottom panel) Derived pseudo-ECG from **pecg3**.

activation sequences are shown for three different pacing RR intervals, 450, 1000, and 1450 ms, leading to the observation that activation times have similar patterns in the three cases. Fig. 7 shows a simulated sequence of isochronic voltage representation during steady-state pacing at 1000 ms, with indication of the timing corresponding to the T-wave peak and T-wave end in the pseudo-ECG from **pecg3**, and of the regions where $\mathrm{APD}_{\mathrm{min}}$ and $\mathrm{APD}_{\mathrm{last}}$ are computed. Since our 2-D preparation includes only transmural heterogeneities, the time instant corresponding to the peak of the T-wave coincides with the time at which complete repolarization of the epicardium occurs, whereas T-wave end coincides with the total repolarization of the tissue. The effect of varying the cell type distribution across the ventricular wall on the isochronic voltage representation at the T-wave peak instant is shown in Fig. 8, for pacing RR intervals of 450, 1000, and 1450 ms. In all isochronic voltage representations, for different pacing rates and cell type distributions, the epicardium is completely repolarized at the T-wave peak instant.

Note that in the simulations shown in Fig. 8, $\mathrm{APD}_{\mathrm{min}}$ remains fixed at different RR levels as needed to apply (3).

An indirect validation of the simulated restitution properties in the 2-D tissue is performed by first comparing steady-state T_{pe}^{dyn} values computed at different RR intervals in tilt test ECGs and in simulated pseudo-ECGs. Fig. 9 shows three regions corresponding to simulations using cell type distributions of 65%/35%, 80%/20% and 90%/10%. Each region represents the range of steady-state $[RR, T_{pe}^{\mathrm{dyn}}]$ curves computed for pseudo-ECGs at eight different sensor positions. The steady-state $[z_{\mathrm{RR}}, T_{pe}]$ curves obtained from the tilt test recordings are superimposed in the same graphic. Note that when the percentages of epi- and midmyocardial cells are more similar (65%/35%), the difference between $\mathrm{APD}_{\mathrm{min}}$ and $\mathrm{APD}_{\mathrm{last}}$ is higher and, therefore, the T_{pe} interval is longer than the ones for 80%/20% and 90%/10% cell type distributions. Simulated values of T_{pe} at different RR intervals for 65%/35% and 80%/20% (default) cell type distributions are found to be within the range

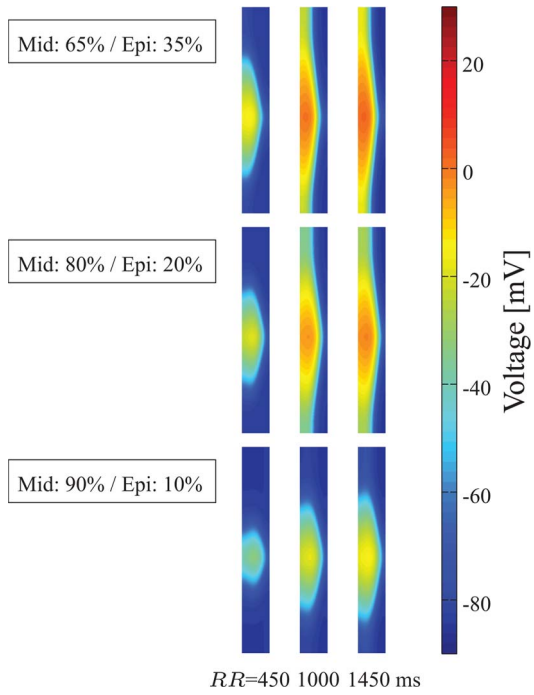

Fig. 8. Isochronic voltage representation at T-wave peak time instant using three different cell type distributions (mid/epi) and pacing RR intervals of 450, 1000, and 1450 ms.

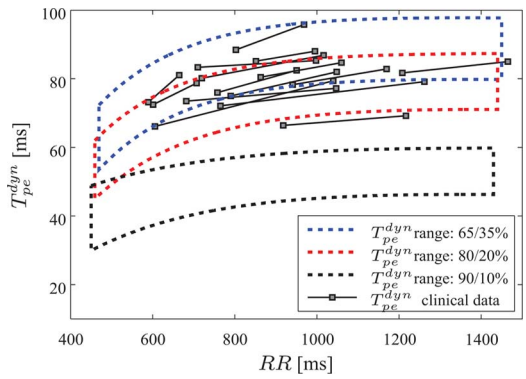

Fig. 9. Steady-state T_{pe}^{dyn} as a function of RR from tilt test recordings (in squares) and from simulations. For the simulations, the regions correspond to cell type distributions of 65%/35%, 80%/20%, and 90%/10%, and each region represents the influence of computing steady-state $[RR, T_{pe}^{\mathrm{dyn}}]$ curves for pseudo-ECGs at different sensor positions.

of values measured from the tilt test recordings. However, simulated T_{pe} values for the 90%/10% percentage are outside the range of the tilt test recordings.

After confirming the good agreement in the repolarization $[RR, T_{pe}^{\mathrm{dyn}}]$ values between pseudo-ECGs and clinical ECGs, the restitution dispersion estimates are also compared. Fig. 10 shows a comparison of pseudo-ECG-based estimates of APDR dispersion, $\widehat{\Delta\alpha}^{\mathrm{pECG}}$, in (12), at sensor positions **pecg3** and **pecg5**, and ECG-based estimates, $\widehat{\Delta\alpha}^{\mathrm{ECG_c}}$, in (9), obtained from the tilt test recordings. Both the average difference between $\widehat{\Delta\alpha}^{\mathrm{pECG}}$ (computed in **pecg3** and **pecg5**) and $\widehat{\Delta\alpha}^{\mathrm{ECG_c}}$, and the average percentage of the difference are shown in

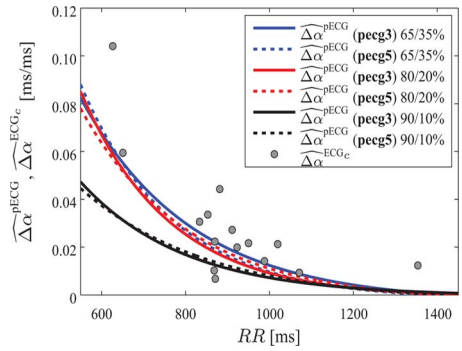

Fig. 10. APDR slope dispersion estimates from the tilt test recordings ($\widehat{\Delta\alpha}^{\mathrm{ECG_c}}$) and from the pseudo-ECGs ($\widehat{\Delta\alpha}^{\mathrm{pECG}}$) derived from two sensor positions (**pecg3** and **pecg5**), and three cell type distributions (mid/epi: 65%/35%, 80%/20%, and 90%/10%).

TABLE I
AVERAGE VALUE ACROSS SUBJECTS OF THE DIFFERENCE BETWEEN THE ESTIMATES MEASURED FROM THE SIMULATED PSEUDO-ECGS IN **PECG3** AND **PECG5** ($\widehat{\Delta\alpha}^{\mathrm{pECG}}$), AND FROM THE TILT TEST RECORDINGS $\widehat{\Delta\alpha}^{\mathrm{ECG_c}}$. DIFFERENT PERCENTAGES OF CELL TYPES HAVE BEEN USED TO DERIVE THE PSEUDO-ECGS

Simulated - Measured	*Cell Percentage*	Average (%) [ms / ms]
$\widehat{\Delta\alpha}^{\mathrm{pECG}}$ (**pecg3**) - $\widehat{\Delta\alpha}^{\mathrm{ECG_c}}$	(65/35%)	-0.0066 (-2%)
	(80/20%)	-0.0100 (-21%)
$\widehat{\Delta\alpha}^{\mathrm{pECG}}$ (**pecg5**) - $\widehat{\Delta\alpha}^{\mathrm{ECG_c}}$	(65/35%)	-0.0090 (-17%)
	(80/20%)	-0.0085 (-11%)

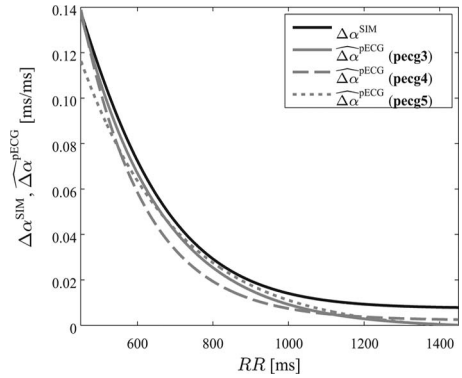

Fig. 11. APDR slope dispersion, $\Delta\alpha^{\mathrm{SIM}}$, for the cell type distribution 80%/20%, and the proposed estimate measured from the pseudo-ECG in **pecg3**, **pecg4**, and **pecg5**.

Table I. Differences are below 20% in mean, which are within physiological variability limits.

B. Assessment of APDR Dispersion Quantified From the Pseudo-ECG

APDR slope dispersion at tissue level, denoted by $\Delta\alpha^{\mathrm{SIM}}$, in (11), has been computed for each of the three cell type distributions. $\Delta\alpha^{\mathrm{SIM}}$ is used to assess whether $\widehat{\Delta\alpha}^{\mathrm{pECG}}$, computed from pseudo-ECGs, is a good estimate of APDR slope dispersion. Fig. 11 shows the comparison between $\Delta\alpha^{\mathrm{SIM}}$ and $\widehat{\Delta\alpha}^{\mathrm{pECG}}$ computed at sensor positions **pecg3**, **pecg4**, and **pecg5** for the default cell type distribution 80%/20%. The error between $\Delta\alpha^{\mathrm{SIM}}$ and $\widehat{\Delta\alpha}^{\mathrm{pECG}}$ from **pecg3** and **pecg5** relative to the slope range is found to be 4% in average, while from **pecg4**, is 6%.

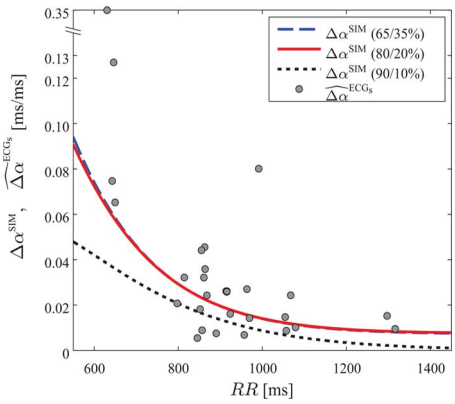

Fig. 12. APDR slope dispersion, $\Delta\alpha^{\mathrm{SIM}}$, computed as a function of RR for three cell type distributions. For each tilt test recording, $\widehat{\Delta\alpha}^{\mathrm{ECG_s}}$ values are shown in circles at the mean of the corresponding RR interval range.

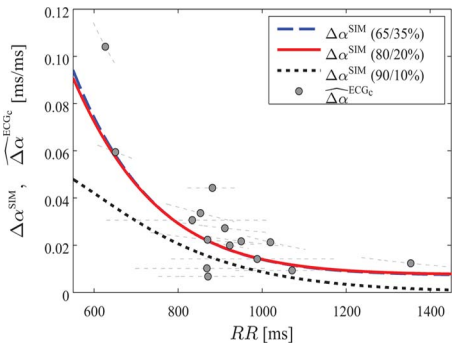

Fig. 13. APDR dispersion, $\Delta\alpha^{\mathrm{SIM}}$, for different cell type distributions as a function of RR. For each tilt test recording, $\widehat{\Delta\alpha}^{\mathrm{ECG_c}}$ values are shown in circles at the mean of the surrogate RR interval range together with the derivative of the optimal $g_k(.,\mathbf{a})$ function over the corresponding RR range.

C. Agreement Between Simulated APDR Dispersion and Estimates From Clinical ECGs

Three stationary ECG segments during the tilt test protocol, corresponding to the end of each stage at supine, standing and back supine positions, are used to compute $\widehat{\Delta\alpha}^{\mathrm{ECG_s}}$. Estimates computed at the mean of the corresponding RR range, are shown in Fig. 12, where they are compared to values of $\Delta\alpha^{\mathrm{SIM}}$, representing simulated APDR slope dispersion at tissue level. Without assuming stationary ECG segments, $\widehat{\Delta\alpha}^{\mathrm{ECG_s}}$ is replaced with $\widehat{\Delta\alpha}^{\mathrm{ECG_c}}$, in which the T_{pe} memory lag is compensated for. A comparison between $\widehat{\Delta\alpha}^{\mathrm{ECG_c}}$ (in circles) and $\Delta\alpha^{\mathrm{SIM}}$ is shown in Fig. 13. The dashed lines depicted in Fig. 13 represent the derivatives of the optimal $g_k(.,\mathbf{a})$ function in the z_{RR} range for each recording. These derivatives evaluated in the mean z_{RR} value are our estimates $\widehat{\Delta\alpha}^{\mathrm{ECG_c}}$. According to the results shown in Figs. 12 and 13, there is a good agreement between simulated

TABLE II
AVERAGE VALUE ACROSS SUBJECTS OF THE DIFFERENCES BETWEEN SIMULATED DISPERSION OF RESTITUTION SLOPES $\Delta\alpha^{\mathrm{SIM}}$ AT TISSUE LEVEL AND THEIR ECG ESTIMATES $\widehat{\Delta\alpha}^{\mathrm{ECG_s}}$ AND $\widehat{\Delta\alpha}^{\mathrm{ECG_c}}$

	Cell Percentage	Average [ms/ms]
$\Delta\alpha^{\mathrm{SIM}} - \widehat{\Delta\alpha}^{\mathrm{ECG_s}}$	(65/35%)	-0.0117 (-29.5%)
$\left(\frac{\Delta\alpha^{\mathrm{SIM}} - \widehat{\Delta\alpha}^{\mathrm{ECG_s}}}{\Delta\alpha^{\mathrm{SIM}}} \cdot 100\right)$	(80/20%)	-0.0119 (-29.5%)
	(90/10%)	-0.0221 (-120.9%)
$\Delta\alpha^{\mathrm{SIM}} - \widehat{\Delta\alpha}^{\mathrm{ECG_c}}$	(65/35%)	-0.0052 (-20.2%)
$\left(\frac{\Delta\alpha^{\mathrm{SIM}} - \widehat{\Delta\alpha}^{\mathrm{ECG_c}}}{\Delta\alpha^{\mathrm{SIM}}} \cdot 100\right)$	(80/20%)	-0.0053 (-19.8%)
	(90/10%)	-0.0137 (-116.8%)

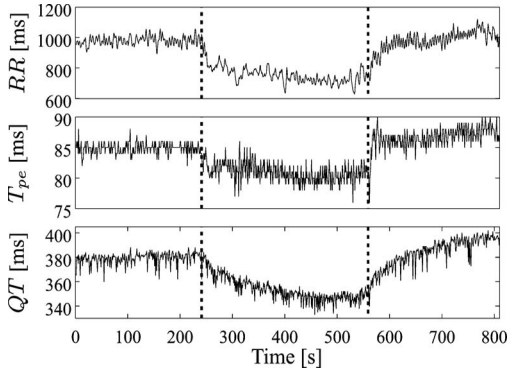

Fig. 14. Rate adaptation of the T_{pe} and QT interval in a tilt test recording showing two abrupt RR changes.

APDR slope dispersion and the ECG estimates $\widehat{\Delta\alpha}^{\mathrm{ECG_s}}$ and $\widehat{\Delta\alpha}^{\mathrm{ECG_c}}$, particulary for $\widehat{\Delta\alpha}^{\mathrm{ECG_c}}$, in which the effects of T_{pe} rate adaptation are compensated for.

Quantification of the results shown in Figs. 12 and 13 is presented in Table II, where average values of the individual differences between simulated $\Delta\alpha^{\mathrm{SIM}}$ and the two ECG estimates, $\widehat{\Delta\alpha}^{\mathrm{ECG_s}}$ and $\widehat{\Delta\alpha}^{\mathrm{ECG_c}}$, are computed. Expressions of those differences as percentages are also included, being 30% in average for $\widehat{\Delta\alpha}^{\mathrm{ECG_s}}$, and 20% for $\widehat{\Delta\alpha}^{\mathrm{ECG_c}}$.

As expected, results for the cell type distribution 90%/10% show higher differences due to the fact that T_{pe} values from the pseudo-ECG are not within the range of our clinical data.

D. T_{pe} Rate Dependence

T_{pe} interval is found to have a very fast adaptation to HR changes as compared to the QT interval. Fig. 14 shows an example of a tilt test recording with two sudden RR changes, to which the T_{pe} interval adapts in a shorter time than the QT interval.

In Fig. 15, left panel, the median, first and third quartile of the T_{pe} adaptation rate, $r(n)$ (see Section II-C), across the 15 recordings are shown and compared to those of the QT interval. In Fig. 15, right panel, an example of the rate adaptation profile $h(n)$ and its cumulative sum $c(n)$ are shown for T_{pe} and QT intervals.

The optimal regression functions $g_k(.,\mathbf{a})$ that characterize the $[z_{\mathrm{RR}}, T_{pe}]$ relationship are found to be linear, $[g_k(z_{\mathrm{RR}}(n),\mathbf{a}) = a_0 + a_1 \cdot z_{\mathrm{RR}}(n)]$, in 33% of the recordings, hyperbolic, $[g_k(z_{\mathrm{RR}}(n),\mathbf{a}) = a_0 + \frac{a_1}{z_{\mathrm{RR}}}(n)]$, in 20%, and hyperbolic tangent, $[g_k(z_{\mathrm{RR}}(n),\mathbf{a})=a_0 + a_1 \cdot \tanh(z_{\mathrm{RR}}(n))]$, in 20%.

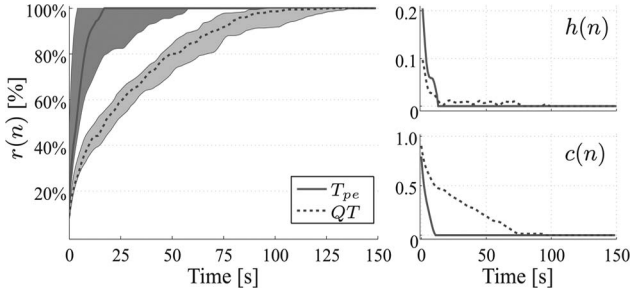

Fig. 15. (Left panel) Median, first and third quartile of the adaptation rates, $r(n)$, of T_{pe} and QT intervals. (Right panel) Example of the adaptation profile, $h(n)$, and its cumulative sum, $c(n)$, for the T_{pe} and QT intervals of a subject undergoing a tilt test protocol.

TABLE III
MEAN ± STD ACROSS SUBJECTS OF THE TIME FOR 90% (t_{90}), 70% (t_{70}), 50% (t_{50}) AND 25% (t_{25}) OF THE COMPLETE RATE ADAPTATION

	QT	T_{pe}
t_{90} (s)	74.1 ± 25.4	23.5 ± 29.7
t_{70} (s)	40.8 ± 15.9	11.4 ± 16.6
t_{50} (s)	19.3 ± 8.9	5.6 ± 7.8
t_{25} (s)	4.2 ± 2.9	1.5 ± 1.9

Table III shows the mean across subjects of the time for 90% (t_{90}), 70% (t_{70}), 50% (t_{50}), and 25% (t_{25}) of the whole T_{pe} rate adaptation. Results are compared to those corresponding to the QT interval.

IV. DISCUSSION

APDR dispersion is considered as an important risk marker in the development of ventricular arrhythmias [7]–[9] and is measured at tissue level. In this study, APDR dispersion, measured at tissue level, has been quantified from the surface ECG, using a novel methodology. To our best knowledge, this is the first time that APDR dispersion is quantified noninvasively by measuring changes in the steady-state T_{pe} with respect to changes in RR interval. First, a 2-D tissue ventricular model has been built and indirectly validated, and the proposed estimate measured at pseudo-ECGs is shown to properly quantify APDR dispersion at tissue level. Then, estimates measured at the acquired ECG recordings are found to be in agreement with the simulated APDR dispersion. Additionally, results from the T_{pe} rate adaptation study show that T_{pe} adapts faster to changes in HR than the QT interval.

A. Evaluation of the 2-D Ventricular Model

We have evaluated the 2-D ventricular tissue model used in this study. First, the underlying model of the 2-D simulation has been reported to reproduce experimentally observed data on APD restitution in single cells from epi, endo, and midmyocardial regions correctly [19], [31]. Characteristics of the 2-D tissue model built in this work, such as dimensions, conduction velocities in the fiber direction [19], and perpendicular to it [25], transmural variation of the fiber angle [26], and heterogeneity

of cell types across the ventricular wall [29], are in agreement with experimental studies. The simulated activation sequence is layered and agrees with the one of an isolated human heart section reported in [27].

Experimental studies in canine wedge preparation [32] show that in case of having transmural heterogeneities only, the time instant of the T-wave peak corresponds to the complete repolarization of the epicardium. This agrees with the results of our 2-D simulations, which include only transmural heterogeneities, where the peak of the T-wave in pseudo-ECGs coincides with the total repolarization of the epicardium in the central part of the tissue (see the isochronic voltage representation in Fig. 7). This has been observed for pacing at different RR intervals and also for different cell type distributions (see Fig. 8).

The APD in the different cell regions of the 2-D tissue slice are within the range of APDs of the subendocardium, midmyocardium, and subepicardium reported in [28].

Steady-state T_{pe}^{dyn} at different RR levels obtained from simulated pseudo-ECGs are in agreement with those measured from ECG control recordings (see Fig. 9). Restitution properties have also been evaluated by comparing the simulated estimations of APDR slope dispersion $\widehat{\Delta\alpha}^{\mathrm{pECG}}$, derived from the pseudo-ECGs, with the values obtained from the tilt test recordings. Results in Table I and Fig. 10 show that simulated values in **pecg3** and **pecg5** are within the range measured in ECG recordings. Sensor positions **pecg3** and **pecg5**, located in the middle part of the tissue, are used to derive $\widehat{\Delta\alpha}^{\mathrm{pECG}}$ due to their similarity to the precordial leads V2, V3, and V4, used to compute the estimates in the tilt test recordings.

B. Assessment of APDR Dispersion Quantified From the Pseudo-ECG

As Fig. 11 shows, $\widehat{\Delta\alpha}^{\mathrm{pECG}}$, measured from the pseudo-ECG provides a quantification of APDR slope dispersion $\Delta\alpha^{\mathrm{SIM}}$ at tissue level, being the mean error relative to the slope range below 6%. This result shows that APDR dispersion at tissue level is properly quantified using the proposed noninvasive estimates.

C. Agreement Between Simulated APDR Dispersion and Estimates From Clinical ECG Data

Two APDR slope dispersion estimates from the surface ECG were proposed: one computed from stationary ECG segments, $\widehat{\Delta\alpha}^{\mathrm{ECG_s}}$; and the other compensating for the T_{pe} hysteresis on RR, $\widehat{\Delta\alpha}^{\mathrm{ECG_c}}$.

In some cases, the estimates $\widehat{\Delta\alpha}^{\mathrm{ECG_s}}$ differ considerable from the $\Delta\alpha^{\mathrm{SIM}}$ values. Reviewing RR trends from those recordings, non stable RR periods are observed. Averaged differences between $\widehat{\Delta\alpha}^{\mathrm{ECG_s}}$ and $\Delta\alpha^{\mathrm{SIM}}$, are of 30% of the value in mean. If we do not assume stable ECG segments and compensate for the T_{pe} memory effect using $\widehat{\Delta\alpha}^{\mathrm{ECG_c}}$, results improve considerably. Averaged differences between $\widehat{\Delta\alpha}^{\mathrm{ECG_c}}$ and $\Delta\alpha^{\mathrm{SIM}}$, which also account for inter subject variability, are of about 20%. If we take into account the individual differences, the averaged difference between $\Delta\alpha^{\mathrm{SIM}}$ and $\widehat{\Delta\alpha}^{\mathrm{ECG_c}}$ is –0.0052, half of the one between $\Delta\alpha^{\mathrm{SIM}}$ and $\widehat{\Delta\alpha}^{\mathrm{ECG_s}}$ (–0.0117). Besides the good agreement between $\Delta\alpha^{\mathrm{SIM}}$ and the corresponding ECG estimates, a similar behaviour with respect to the RR values is observed. Also, our results are in accordance with the slope values reported in [18] for healthy subjects.

The estimate $\widehat{\Delta\alpha}^{\mathrm{ECG_c}}$ shows promising results to extend this method to evaluate arrhythmic pathologies related to restitution dispersion.

D. T_{pe} Rate Adaptation

There are clinical studies which suggest T_{pe} to be practically independent of HR [17], while other studies claim that it is markedly rate dependent [18]. An argument in favor of T_{pe} to be rate dependent is that T_{pe} interval accounts for differences of APDs in different cell regions and APDs are known to be rate related [15]. In this study, T_{pe} rate adaptation has been characterized, showing that it has a short memory lag.

T_{pe} takes about 25 s in mean to complete 90% of its rate adaptation and only 11 s to complete 70% of the whole adaptation. This is in contrast to QT rate adaptation, which has a pronounced memory effect, with about 74 s to complete 90% of its rate adaptation. However, this t_{90} value of 74 s in mean for the QT adaptation is lower than the t_{90} reported in [33], which is around 120 s. This may be due, among other reasons, to the younger age of the control subjects of the tilt test database used in this study. While T_{pe} dependence on a previous history of RR intervals presents a fast decay in one phase, in the case of the QT interval, the decay is performed in two phases, a fast one and a slow one, in concordance with observations from previous studies [15].

APD in ventricular myocytes (epi, mid, and endocardial cells) are known to have a slow adaptation [15], which is performed in two phases: a fast initial one and a subsequent slow one. In [34], APD has been shown to require around 2 min in midmyocardial cells, and 3 min in epicardial cells, to reach a new steady state after a step HR change. However, while the fast phases of APD rate adaptation are different in both cell types, with midmyocardial cells presenting faster decay than epicardial cells, they do have similar slow phases. Therefore, measures such as T_{pe}, which accounts for contributions of different cell types, would not have slow phase (it has been compensated) and the fast phase would include the maximum difference among the fast phases of the different cells in the tissue.

V. Limitations of the Study

The 2-D simulation does not incorporate a 3-D geometry of a left ventricle wall to compute APDR dispersion. Also, heterogeneities other than transmural ones, e.g., apex to base, were not included, which could shed light on the understanding of the T_{pe}. Those considerations could have led to different sites associated with $\mathrm{APD_{min}}$ and $\mathrm{APD_{last}}$, as described after (1). However, they would not imply any change in our methodology. Also, it is worth mentioning that the dispersion quantified in our

study is that accounted for by the T_{pe} interval, which does not necessarily correspond to the maximum dispersion in the tissue.

Healthy subjects have been used to evaluate the proposed methodology to noninvasively quantify restitution dispersion. The next step will be to apply the methodology to estimate restitution dispersion in patients who experienced VT or VF and compare it with control subjects.

Tilt test recordings were obtained from subjects aged 25 to 33 years old with no previous history of cardiovascular disease. However, the data used for the development of the human ventricular action potential model used in this study are not always specific of young healthy hearts.

When characterizing T_{pe} rate adaptation, differences in HR accelerations and decelerations have not been accounted for. In the case of the QT interval or the APD, rate adaptation has been shown to be longer after HR decelerations than after HR accelerations [15], [34].

VI. Conclusion

APDR dispersion has been suggested to play an important role in the development of ventricular arrhythmias. In this study, a method to estimate dispersion of APDR slope curves by making only use of the surface ECG was developed. The proposed ECG-based estimate was evaluated on tilt test recordings of healthy subjects, and showed very good agreement with dispersion of APDR slopes at tissue level, computed using an electrophysiologically detailed human ventricular model. The proposed estimate accounts for the T_{pe} memory lag after HR changes, which was shown to be faster than that of the QT interval.

References

[1] D. S. Rosenbaum, L. E. Jackson, J. M. Smith, H. Garan, J. N. Ruskin, and C. R. J., "Electrical alternans and vulnerability to ventricular arrhythmias," *N. Engl. J. Med.*, vol. 330, no. 4, pp. 235–241, 1994.

[2] M. L. Koller, M. L. Riccio, and R. F. Gilmour Jr., "Dynamic restitution of action potential duration during electrical alternans and ventricular fibrillation," *Amer. J. Physiol. Heart Circ. Physiol.*, vol. 275, pp. 1635–1642, 1998.

[3] M. R. Franz, C. D. Swerdlow, L. B. Liem, and J. Schaefer, "Cycle length dependence of human action potential duration in vivo," *J. Clin. Invest.*, vol. 82, pp. 972–979, 1988.

[4] M. L. Riccio, M. L. Koller, and R. F. Gilmour Jr., "Electrical restitution and spatiotemporal organization during ventricular fibrillation," *Circ. Res.*, vol. 84, pp. 955–963, 1999.

[5] R. J. Selvaraj, P. Picton, K. Nanthakumar, and V. S. Chauhan, "Steeper restitution slopes across right ventricular endocardium in patients with cardiomyopathy at high risk of ventricular arrhythmias," *Amer. J. Physiol. Heart Circ. Physiol.*, vol. 292, pp. 1262–1268, 2007.

[6] K. R. Laurita, S. D. Girouard, and D. S. Rosenbaum, "Modulation of ventricular repolarization by a premature stimulus: Role of epicardial dispersion of repolarization kinetics demonstrated by optical mapping of the intact guinea pig heart," *Circ. Res.*, vol. 79, pp. 493–503, 1996.

[7] M. Nash, C. Bradley, P. Sutton, R. Clayton, P. Kallis, M. Hayward, D. Paterson, and P. Taggart, "Whole heart action potential duration restitution properties in cardiac patients: a combined clinical and modelling study," *Exp. Physiol.*, vol. 91, no. 2, pp. 339–354, 2006.

[8] R. Coronel, F. J. G. Wilms-Schopman, T. Opthof, and M. J. Janse, "Dispersion of repolarization and arrhythmogenesis," *Heart Rhythm*, vol. 6, no. 4, pp. 537–543, 2009.

[9] H. Pak, S. Hong, G. Hwang, H. Lee, S. Park, J. Ahn, Y. Moo Ro, and Y. Kim, "Spatial dispersion of action potential duration restitution kinetics is associated with induction of ventricular tachycardia/fibrillation in humans," *J. Cardiovasc. Electrophysiol.*, vol. 15, no. 12, pp. 1357–1363, 2004.

[10] A. M. Yue, M. R. Franz, P. R. Roberts, and J. M. Morgan, "Global endocardial electrical restitution in human right and left ventricles determined by noncontact mapping," *J. Amer. Coll. Cardiol.*, vol. 46, pp. 1067–1075, 2005.

[11] C. Antzelevitch, W. Shimizu, G. Yan, S. Sicouri, J. Weissenburger, V. Nesterenko, A. Burashnikov, J. Di Diego, J. Saffitz, and G. Thomas, "The M cell: Its contribution to the ECG and to normal and abnormal electrical function of the heart," *J. Cardiovasc. Electrophysiol.*, vol. 10, pp. 1124–1152, 1999.

[12] T. Opthof, R. Coronel, F. J. G. Wilms-Schopman, A. N. Plotnikov, I. N. Shlapakova, P. Danilo, M. R. Rosen, and M. J. Janse, "Dispersion of repolarization in canine ventricle and the electrocardiographic T wave: Tp-e interval does not reflect transmural dispersion," *Heart Rhythm*, vol. 4, no. 3, pp. 341–348, 2007.

[13] Y. Xia, Y. Liang, O. Kongstad, Q. Liao, M. Holm, B. Olsson, and S. Yuan, "In vivo validation of the coincidence of the peak and end of the T wave with full repolarization of the epicardium and endocardium in swine," *Heart Rhythm*, vol. 2, no. 2, pp. 162–169, 2005.

[14] E. Pueyo, P. Smetana, P. Caminal, Bayes, M. Malik, and P. Laguna, "Characterization of QT interval adaptation to RR interval changes and its use as a risk-stratifier of arrhythmic mortality in amiodarone-treated survivors of acute myocardial infarction," *IEEE Trans. Biomed. Eng.*, vol. 51, no. 9, pp. 1511–1520, Sep. 2004.

[15] C. P. Lau, A. R. Freedman, S. Fleming, M. Malik, A. J. Camm, and D. E. Ward, "Hysteresis of the ventricular paced QT interval in response to abrupt changes in pacing rate," *Cardiovasc. Res.*, vol. 22, pp. 67–72, 1988.

[16] E. Pueyo, M. Malik, and P. Laguna, "A dynamic model to characterize beat-to-beat adaptation of repolarization to heart rate changes," *Biomed. Signal Process. Control*, vol. 3, pp. 29–43, 2008.

[17] M. P. Andersen, J. Q. Xue, C. Graff, J. K. Kanters, E. Toft, and J. J. Struijk, "New descriptors of T-wave morphology are independent of heart rate," *J. Electrocardiol.*, vol. 41, no. 6, pp. 557–561, 2008.

[18] P. Smetana, V. Batchvarov, K. Hnatkova, A. J. Camm, and M. Malik, "Sex differences in the rate dependence of the T wave descending limb," *Cardiovasc. Res.*, vol. 58, no. 3, pp. 549–554, 2003.

[19] K. Ten Tusscher and A. Panfilov, "Alternans and spiral breakup in a human ventricular tissue model," *Amer. J. Physiol. Heart Circ. Physiol.*, vol. 291, no. 3, pp. H1088–H1100, 2006.

[20] J. P. Martínez, R. Almeida, S. Olmos, A. P. Rocha, and P. Laguna, "A wavelet-based ECG delineator: Evaluation on standard databases," *IEEE Trans. Biomed. Eng.*, vol. 51, no. 4, pp. 570–581, Apr. 2004.

[21] Z. Qu, J. N. Weiss, and A. Garfinkel, "Cardiac electrical restitution properties and stability of reentrant spiral waves: a simulation study," *Amer. J. Physiol. Heart Circ. Physiol.*, vol. 276, pp. 269–283, 1999.

[22] P. C. Hansen, "Analysis of discerte ill-posed problems by means of the L-curve," *SIAM Rev.*, vol. 34, no. 4, pp. 561–580, 1992.

[23] J. Nocedal and S. Wright, *Numerical Optimization*. New York: Springer-Verlag, ch. 6, pp. 135–143.

[24] E. Heidenreich, J. M. Ferrero, M. Doblaré, and J. F. Rodríguez, "Adaptive macro finite elements for the numerical solution of monodomain equations in cardiac electrophysiology," *Ann. Biomed. Eng.*, vol. 38, pp. 2331–2345, 2010.

[25] G.-X. Yan, W. Shimizu, and C. Antzelevitch, "Characteristics and distribution of M cells in arterially perfused canine left ventricular wedge preparations," *Circulation*, vol. 98, pp. 1921–1927, 1998.

[26] D. D. Streeter, H. M. Spotnitz, D. P. Patel, J. Ross, and E. H. Sonnenblick, "Fiber orientation in the canine left ventricle during diastole and systole," *Circ. Res.*, vol. 24, pp. 339–347, 1969.

[27] D. Durrer, R. T. van Dam, G. E. Freud, M. J. Janse, F. L. Meijler, and R. C. Arzbaecher, "Total excitation of the isolated human heart," *Circulation*, vol. 41, pp. 899–912, 1970.

[28] A. V. Glukhov, V. V. Fedorov, Q. Lou, V. K. Ravikumar, P. W. Kalish, R. B. Schuessler, N. Moazami, and I. R. Efimov, "Transmural dispersion of repolarization in failing and nonfailing human ventricle," *Circ. Res.*, vol. 106, no. 5, pp. 981–991, 2010.

[29] E. Drouin, F. Charpentier, C. Gauthier, K. Laurent, and H. Le-Marec, "Electrophysiologic characteristics of cells spanning the left ventricular wall of human heart: Evidence for presence of M cells," *Amer. J. Physiol. Heart Circ. Physiol.*, vol. 26, no. 1, pp. 185–192, 1995.

[30] K. Gima and Y. Rudy, "Ionic current basis of electrocardiographic waveforms: A model study," *Circ. Res.*, vol. 90, pp. 889–896, 2002.

[31] K. Ten Tusscher, D. Noble, P. J. Noble, and A. Panfilov, "A model for human ventricular tissue," *Amer. J. Physiol. Heart Circ. Physiol.*, vol. 286, pp. H1573–H1589, 2004.

[32] G. Yan and C. Antzelevitch, "Cellular basis for the normal T wave and the electrocardiographic manifestations of the long-qt syndrome," *Circulation*, vol. 98, pp. 1928–1936, 1998.
[33] E. Pueyo, J. P. Martínez, and P. Laguna, "Cardiac repolarization analysis using the surface electrocardiogram," *Phil. Trans. R. Soc. A*, vol. 367, pp. 213–233, 2009.
[34] E. Pueyo, Z. Husti, T. Hornyik, I. Baczkó, P. Laguna, A. Varró, and B. Rodríguez, "Mechanisms of ventricular rate adaptation as a predictor of arrhythmic risk," *Amer. J. Physiol. Heart Circ. Physiol.*, vol. 298, pp. 1577–1587, 2010.

Ana Mincholé received the M.Sc. degree in physics from the University of Zaragoza, Zaragoza, Spain, in 2002, and received the the Masters degree in nanoscale physics and engineering from Chalmers University of Technology, Göteborg, Sweden. In 2011, she obtained the Ph.D. degree in biomedical engineering at the University of Zaragoza.

She is currently with the Centro de Investigación Biomédica en Red en Bioingeniería, Biomateriales y Nanomedicina (CIBER-BBN), University of Zaragoza. Her current research interests include biomedical signal processing, especially in automatic detection of ischemia in ambulatory recordings, and the search for arrhythmic risk markers from the electrocardiographic signal.

Esther Pueyo received the M.S. degree in mathematics from the University of Zaragoza, Zaragoza, Spain, in 1999.

During 2000, she was a Research Student in the Department of Mathematics, University of Zaragoza, where she developed a minor thesis in the field of Calculus. In 2001, she started her Ph.D. studies in biomedical engineering at the University of Zaragoza, with a grant supported by the Spanish government. She was also an Assistant Professor in the field of signal processing. She was engaged in developing signal processing techniques applied to the electrocardiogram with the purpose of investigating abnormal conditions that lead to the genesis of malignant cardiac arrhythmias. She is currently an Associate Professor in the Department of Electronic Engineering and Communications, University of Zaragoza. Her current research interests include investigating the mechanisms of arrhythmic risk, either drug-induced or due to pathological effects, with the aim of providing new selective biomarkers that can help to improve diagnosis of cardiac diseases.

José Felix Rodríguez received the B.E. degree in mechanical engineering from the Universidad Simón Bolívar, Bolívar, Venezuela, in 1993, and the Ph.D. degree in mechanical engineering from the University of Notre Dame, IN, in 1999.

He is currently an Associate Research Professor at the Institute for Engineering Research (I3A), Universidad de Zaragoza, Zaragoza, Spain, and in the Department of Mechanical Engineering, coordinating the research line in biophysics and cardiac mechanics in the Structures and Material Modeling Group hosted by I3A. His current research interests include vascular biomechanics, cardiac electrophysiology, and cell mechanics.

Ernesto Zacur received the M.Sc. degree in physics from the Instituto Balseiro, Balseiro, Argentina, in 2003. He is currently working toward the Ph.D. degree in biomedical engineering at the Aragón Institute for Engineering Research (I3A), University of Zaragoza, Zaragoza, Spain.

From 2004 to 2006, he was an Assistant Professor at the Pompeu Fabra University, Spain. His current research interests include mathematical tools for image analysis, specially those related to large deformation image registration, and their applications to the analysis of medical images.

Manuel Doblaré was born in Córdoba, Spain, in July 1956. He received the Mechanical and Electrical Engineering degree from the University of Seville (SU), Seville, Spain, in 1978, ranking #1.

From 1978 to 1982, he was a Research Assistant at SU and PUM, when he got the position of an Assistant Professor of structural mechanics at the latter. Since 1984, he has been a Full Professor in the Department of Mechanical Engineering, University of Zaragoza (ZU), Zaragoza, Spain. He was a Visiting Scholar in the Department of Civil Engineering, Universities of Southampton (1981) and Courant Institute of Mathematical Sciences, New York (1983), and a Visiting Professor at Division of Applied Mechanics, Stanford University (1990). He joined the Ph.D. programme of the Polytechnic University of Madrid (PUM) in 1979, presenting the Ph.D. dissertation in 1981. He is a member of different national and international scientific associations, a member of the Editorial Board of several international journals, and a member of the Spanish Royal Academy of Engineering and the Royal Academy of Mathematics, Physics, Chemistry, and Natural Sciences of Zaragoza. He was the Head of the Department, the Dean of the Faculty of Engineering of the University of Zaragoza, the Director of the Aragón Institute for Engineering Research (I3A), and a member of different national and European Commissions related to research. He is currently the Director of the Spanish Networking Center on Bioengineering, Biomaterials and Nanomedicine (CIBER-BBN). His current research interests include computational solid mechanics with applications to structural integrity, biomechanics, and mechanobiology, and the development and FE implementation of constitutive models for hard and soft tissues, interaction between tissues and biomaterials, and mechanobiological models for cellular processes.

Dr. Doblaré has received several prizes including the 2008 Aragón Prize to Excellence in Research, a "Honoris Causa" Doctorate by the University of Cluj-Napoca, Romania. He received the prizes of the PUM and the "Artigas Foundation" for the best Ph.D. thesis in mechanical engineering in 1981.

Pablo Laguna was born in Jaca, Huesca, Spain, in 1962. He received the M.S. degree in physics and the Ph.D. degree in physic science from the Science Faculty, University of Zaragoza, Zaragoza, Spain, in 1985 and 1990, respectively.

The Ph.D. thesis was developed at the Biomedical Engineering Division, Institute of Cybernetics (U.P.C.-C.S.I.C.), under the direction of Pere Caminal. He is currently a Full Professor of signal processing and communications in the Department of Electrical Engineering, Engineering School, and a Researcher at the Aragón Institute for Engineering Research (I3A), both at University of Zaragoza, Spain. He is also a member of the Spanish Center for Biomedical Engineering, Biomaterial and Nanomedicine Research CIBER-BBN, where from 1992 to 2005, he was an Associate Professor. From 1987 to 1992, he was an Assistant Professor of automatic control in the Department of Control Engineering, Politecnic University of Catalonia (U.P.C.), Spain, and a Researcher in the Biomedical Engineering Division, Institute of Cybernetics (U.P.C.-C.S.I.C.). His current research interests include signal processing, in particular applied to biomedical applications. He has coauthored more than research 70 papers on this topic. He is, together with L. Sörnmo, the author of *Bioelectrical Signal Processing in Cardiac and Neurological Applications* (Elsevier, 2005).